TSINGHUA SCIENCE AND TECHNOLOGY
ISSN 1007-0214 17/32 pp695–707
DOI: 10.26599/TST.2023.9010129
Volume 30, Number 2, April 2025

A Fall Detection Device Based on Single Sensor Combined with Joint Features

Li Zhang*, Yu-An Liu*, Qiuyu Wang, Huilin Chen, Jingao Xu, and Danyang Li

Abstract: Accidental falls pose a significant threat to the well-being of the elderly, thus facilitating a quantum leap in the field of fall detection technology. For fall detection, accurate identification of fall behavior is a key priority. Our study proposes an innovative methodology to detect falls during activities of daily living (ADL), with the objective of preventing further harm. Our design aims to achieve precise identification of falls by extracting a variety of features obtained from the simultaneous acquisition of acceleration and angular velocity data using a single sensor. To enhance detection accuracy and reduce false alarms, we establish a classifier based on the joint acceleration and Euler angle feature (JAEF) analysis. With the aid of a support vector machine (SVM) classifier, human activities are classified into eight categories: going upstairs, going downstairs, running, walking, falling forward, falling backward, falling left, and falling right. In particular, we introduce a novel approach to enhance the accuracy of fall detection algorithms by introducing the Equal Signal Amplitude Difference method. Through experimental demonstration, the proposed method exhibits a remarkable sensitivity of 99.25%, precision of 98.75%, and excels in classification accuracy. It is noteworthy that the utilization of multiple features proves more effective than relying solely on a single aspect. The preliminary findings highlight the promising applications of our study in the field of fall injury systems.

Key words: fall detection; support vector machine; wearable sensor; activity recognition

1 Introduction

The phenomenon of falls represents a momentous threat to the elderly and disabled population, often acknowledged as the "fatal killer"[1]. Recent empirical evidence from the Centers for Disease Control and Prevention reveals that no less than 25% of individuals aged 65 and above encounter incidents of falling on an annual basis[2]. It is pertinent to note that falls can be classified into four fundamental types, comprising falling forward, falling backward, falling left, and falling right[3]. Clinical studies underscore the importance of precise, rapid, and robust multi-directional fall detection. This aids clinicians in promptly identifying the injured joint and minimizing fall-related damage. Multi-directional data can shed light on the most likely site of the initial head hit, especially in cases of cerebral hemorrhage and brain damage.

Therefore, the precise and expeditious identification of falls occurring in multiple directions necessitates the utilization of specific and efficacious techniques. We studied numerous posture estimation-based or human motion-induced improved methods in ambient signal-detecting systems for falls. Currently, most fall detection systems can only determine the incidence of

• Li Zhang, Yu-An Liu, Qiuyu Wang, and Huilin Chen are with School of Mathematics, Hefei University of Technology, Hefei 230009, China. E-mail: lizhang@hfut.edu.cn; yuanliu@gmail.com; 2020111428@mail.hfut.edu.cn; 2021111448@mail.hfut.edu.cn.
• Jingao Xu and Danyang Li are with School of Software and also with BNRist, Tsinghua University, Beijing 100084, China. E-mail: xujingao13@gmail.com; lidanyang1919@gmail.com.
* To whom correspondence should be addressed.
Manuscript received: 2023-04-20; revised: 2023-10-17; accepted: 2023-10-29

a fall, usually divided into two different categories.

(1) Environmental device-based systems, like radar[4], microphone[5], radio-frequency devices[6], cameras[7], and multimodal approach[8], detect fall activity largely by the deployment of particular detection modules. The primary limitation of wearable technology resides in its limited perspective. Additionally, the use of cameras in this context raises concerns about potential infringements on personal privacy.

(2) Wearable technology captures both translational and rotational movements on the body through miniature sensors, enabling the detection of falls[9–11]. Its portability and ubiquitous computing capabilities are notable advantages.

To achieve exact fall detection, pose signals or environmental signals are employed. Lai et al.[12] used six accelerometers distributed throughout the body to accurately measure various postures and identify accidental falling episodes. Nevertheless, this approach lacks the capacity to determine the direction of descent. Wang et al.[13] proposed a real-time contactless fall detection system using common WiFi devices. The limitations of vision-based posture estimation methods lie in the constraints posed by flexibility and available space. Furthermore, these methods often rely on individual scenarios and varying conditions.

Recent studies have highlighted the efficacy of wearable technology in the detection and recognition of incidents involving falls. Lu et al.[14] created an energy-saving barometer with a maximum specificity of 98.0% and a maximum sensitivity of 96.1% for detecting falls. Montanini et al.[15] and de Quadros et al.[16] used smart shoes with several sensors and a wristband, respectively, to detect falls based on the threshold fall detection approach. On the contrary, these fall detection methods require the extraction of intricate data attributes from a multitude of sensors, encompassing components such as accelerometers and gyroscopes. Moreover, these techniques require significant allocation of training and computational resources.

2 Related Work

In the current detection method of falls before the collision, Nyan et al.[17] discovered falls by analyzing the angle and angular velocity of the thigh in various falls and daily activities. Shi et al.[18], and Shan and Yuan[19] used support vector machine (SVM) to extract features collected by accelerometers and gyroscopes to discover the fall. Wu and Xue[20] and Bourke et al.[21] used the vertical velocity characteristics of the human body in descending stage to detect descending, which requires using data from accelerometers and gyroscopes to calculate vertical velocity. Gao et al.[22] fixed four sensors to the waist, thigh, chest, and sides of the body to detect falls. Nyan et al.[23] discovered falls by evaluating data correlations between thigh and waist. Wang et al.[24] saw and processed wireless signal channel state information (CSI) data and identified abnormal CSI sequences using local outlier factor technology. Nevertheless, these methods of fall detection suffer from the following limitations: (1) Relying on thresholds to discern between falls and activities of daily living (ADL) poses difficulties in adapting to dynamic fluctuations in the environment. (2) The utilization of numerous sensors to gather data introduces intricacy and reduces overall versatility.

Conventional classification methods have been widely utilized in the domains of fall detection and activity recognition[25]. A neural network was proposed by Ref. [26] to recognize falls and non-falls. Yu et al.[27] developed a video image processing-based online SVM algorithm to acknowledge falls. Shen et al.[28] developed a high-level fuzzy Petri net-based fall detection system. They placed the smartphone in their thigh pocket for fall protection while studying. Real-world situations can present particular challenges. To exemplify, while walking, the positional relationship of a smartphone remains variable and showcases a stochastic characteristic. Hence, it requires the utilization of genuine training data to construct a resilient mathematical model. The authors suggested a system for detecting falls based on several classifiers[29]. The algorithm was developed using artificial neural networks (ANN), k-nearest neighbors (KNN), radial basis functions (RBF), probabilistic principal component analyses (PPCA), and linear discriminant analyses (LDA). It is unsuitable for wearable electronics. Regardless of the positive outcome, classification procedures are frequently time-consuming. Researchers typically favor more straightforward techniques for pre-impact fall detection systems. Tong et al.[30] proposed a hidden Markov model-based fall-prediction approach which can anticipate 200–400 ms before impact. Liu and Lockhart[31] used forecast classifier analysis to create a fall detection method before a crash. The average

response time for the program to detect backward falls was 255 ms.

By reason of the foregoing, this study seeks to explore the suitability of the SVM-based fall detection system. To achieve dependable differentiation between fall actions and ADLs, our focus lies on the construction of feature vectors, extraction of features, and implementation of classification techniques. These approaches aim to optimize the accuracy of identification. This paper is an extension of our conference paper accepted by MWSSH2022[32]. The following is a summary of the significant contributions:

(1) We present a robust methodology for extracting discerning features that enable differentiation among various activities, utilizing the SVM to discriminate between falls and ADLs.

(2) We develop an innovative signal processing technique to capture Euler angular data, which undergoes meticulous filtering to enhance the resolution of the extracted features.

(3) We produce abundant investigations to substantiate that an IMU device suffices to attain exceptional precision in discriminating different motion patterns

3 System Overview

The system architecture is depicted in Fig. 1, showcasing the comprehensive framework. The SVM receives training data using the features derived from the IMU dataset. Concurrently, the user's IMU captures data across six axes, transmitting the processed features to the server. Initially, the user records ADLs and fall events using the inertial sensor embedded within the system. Subsequently, the server receives the streams of acceleration and angular velocity data to establish an enhanced training framework. Based on this foundation, the data streams are segmented, features are extracted, and a fuzzy query is performed on the angle feature matrix. Ultimately, the SVM undergoes training with the obtained results. To achieve a relatively accurate prediction outcome, the user examines both the acceleration and angular velocity data collected from the IMU within the system, transmitting them into the SVM model. Should the system identify a fall incident, it promptly activates the user's alarm device, ensuring timely care or emergency treatment for the elderly.

3.1 Hardware

Figure 2 shows the hardware for the fall detection system includes a sensor (MPU6050), secured to the body with a bandage. Our research focuses on the most general criterion of falls with backward, forward, left, and right falls during ADLs. In the standing posture, angular velocity and acceleration values are near to 0 °/s and 9.79 m/s^2 after calibration. The module possesses the capability to generate real-time data in a dynamic environment. A Bluetooth connection is employed to transfer the sampled data to either a personal computer or a smartphone, ensuring seamless communication.

3.2 Data preprocessing

For a fall detection system, the primary task of utmost importance is to extract appropriate features from the collected data in order to accurately characterize falling behavior. The distinction from the majority of recent studies, this paper adopts a machine learning approach.

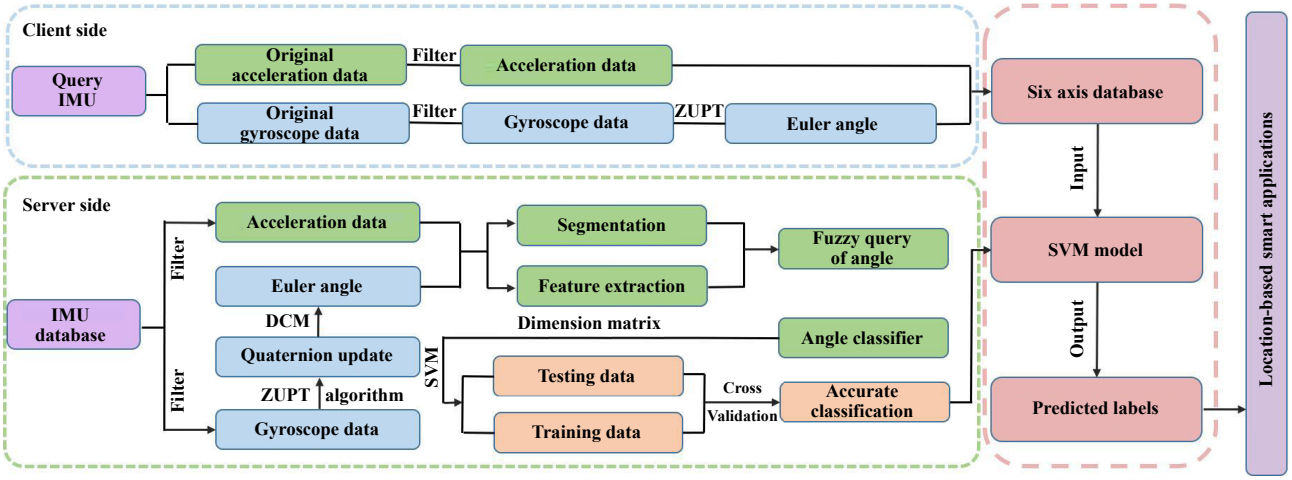

Fig. 1 Overview of system.

Fig. 2 IMU device.

The SVM's training accuracy is significantly increased in this paper by combining accelerations and Euler angles as training features. Moreover, a zero-velocity updating technique is used to obtain Euler angles. An appropriate coordinate framework should be selected to effectively describe the spatial motion state of the carrier. Assume that Fig. 3 represents both the navigational coordinate framework (the N framework) and the body coordinate framework (the B framework). The fundamental rotations from the N framework to the first rotational framework, the first rotational framework to the second rotational framework, and the second rotational framework to the B framework, respectively, are denoted by the letters C_n^1, C_1^2, and C_2^b. The coordinate transformation matrix, C_b^n, from the N system to the B system is thus written as

$$C_2^b = \begin{bmatrix} 1 & 0 & 0 \\ 0 & \cos\gamma & \sin\gamma \\ 0 & -\sin\gamma & \cos\gamma \end{bmatrix} \tag{1}$$

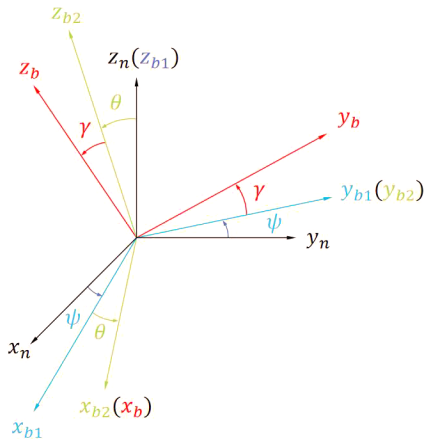

Fig. 3 Transformation of sensor space angle position.

$$C_1^2 = \begin{bmatrix} \cos\theta & 0 & -\sin\theta \\ 0 & 1 & 0 \\ \sin\theta & 0 & \cos\theta \end{bmatrix} \tag{2}$$

$$C_n^1 = \begin{bmatrix} \cos\psi & \sin\psi & 0 \\ -\sin\psi & \cos\psi & 0 \\ 0 & 0 & 1 \end{bmatrix} \tag{3}$$

An orthogonal matrix is used to transform two Cartesian coordinate frameworks. Thus, it yields

$$C_b^n = \left(C_n^b\right)^{-1} = \left(C_n^b\right)^{\mathrm{T}} \tag{4}$$

$$C_b^n = \begin{bmatrix} \cos\psi\cos\theta & C_{12} & C_{13} \\ \cos\theta\sin\psi & C_{22} & C_{23} \\ -\sin\theta & \sin\gamma\cos\theta & \cos\theta\cos\gamma \end{bmatrix} \tag{5}$$

where the matrix C_b^n is used to convert coordinates from the B framework to the N framework, and

$$\begin{aligned} C_{12} &= \sin\gamma\sin\theta\cos\psi - \cos\gamma\sin\psi, \\ C_{13} &= \sin\gamma\sin\psi + \cos\gamma\sin\theta\cos\psi, \\ C_{22} &= \cos\psi\sin\gamma + \sin\gamma\sin\theta\sin\psi, \\ C_{23} &= \sin\psi\sin\theta\cos\gamma - \sin\gamma\cos\psi \end{aligned} \tag{6}$$

Using the measurement from the IMU, the system's attitude updating process involves calculating matrix C_b^n in real-time. The symbol ω_{nb} represents the angular speed of the B framework in relation to the N system. The parts of ω_{nb} in the B system are then listed as follows:

$$\begin{bmatrix} \omega_{nbx}^b \\ \omega_{nby}^b \\ \omega_{nbz}^b \end{bmatrix} = C_2^b C_1^2 \begin{bmatrix} 0 \\ 0 \\ -\psi \end{bmatrix} + C_2^b \begin{bmatrix} 0 \\ \theta \\ 0 \end{bmatrix} + \begin{bmatrix} \gamma \\ 0 \\ 0 \end{bmatrix} \tag{7}$$

Then, the Euler angle differential equation is produced as follows:

$$\begin{bmatrix} \gamma \\ \theta \\ \psi \end{bmatrix} = \begin{bmatrix} 1 & 0 & -\sin\theta \\ 0 & \cos\gamma & \sin\gamma\cos\theta \\ 0 & -\sin\gamma & \cos\gamma\cos\theta \end{bmatrix}^{-1} \begin{bmatrix} \omega_{nbx}^b \\ \omega_{nby}^b \\ \omega_{nbz}^b \end{bmatrix} \tag{8}$$

Regarding ADLs, the relative positions of the three Euler angular axes exhibit minimal variations. However, during a falling event, notable changes in these positions occur, making them distinguishable. The Euler angle, therefore, serves as a discriminative factor between falling actions and ADLs.

When the person falls four times during walking, Fig. 4 depicts the change in the Euler angle. The signals that the accelerometer and gyroscope need to be cleaned of noise. Hence, averaging filters are employed to attenuate noise present in the acceleration and Euler angle signals, resulting in smoother and more refined

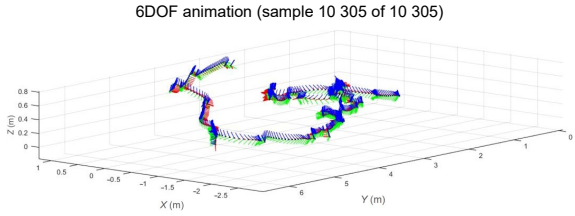

Fig. 4 Pedestrians experienced falls while walking.

data. The acceleration and Euler angle values are transmitted over Bluetooth to a PC, and then recorded by a recording application for analysis.

3.3 Windowing technique (Sliding window)

As mentioned earlier, the process of noise filtering involves partitioning the accelerated data into several smaller segments, each with a predetermined size. To ensure minimal loss of data samples, a sliding window approach is implemented, with a carefully chosen overlapping ratio. This strategy helps maintain a high recognition rate for activities. It is important to note that each action possesses distinct characteristics, necessitating the scaling of the data window size in a tailored manner, thereby facilitating accurate identification of activity classes. Figure 5 depicts the data flow on acceleration under various windows. Although it is less effective in suppressing interference points, it can assist in the detection of quick activities in shorter windows. For extended windows, it can reduce interference more effectively, while it also distorts the signal. Therefore, it is crucial to determine the appropriate window size, evaluate sliding window parameters, and reliably detect the impact of falling behavior on recognition performance.

3.4 Features extraction algorithm

Extraction of the proper features from the gathered data is crucial for accurate fall recognition. Figure 6 shows the acceleration waveforms for each action. As apparent, each acceleration waveform possesses unique characteristics. The time interval between each step was relatively longer for upstairs and downstairs, and the change in wave amplitude was greater for downstairs compared to upstairs. Running and walking exhibited the briefest temporal intervals per step, with running further demonstrating a reduced inter-step time interval. However, the left, right, forward, and backward falls are characterized by a step change in acceleration in at least one direction compared to the other four movements, in addition to the different directions and magnitudes between the four movements of the fall. Figure 7 shows the Euler angular waveforms for each action. The main differences between the waveforms for walking up and

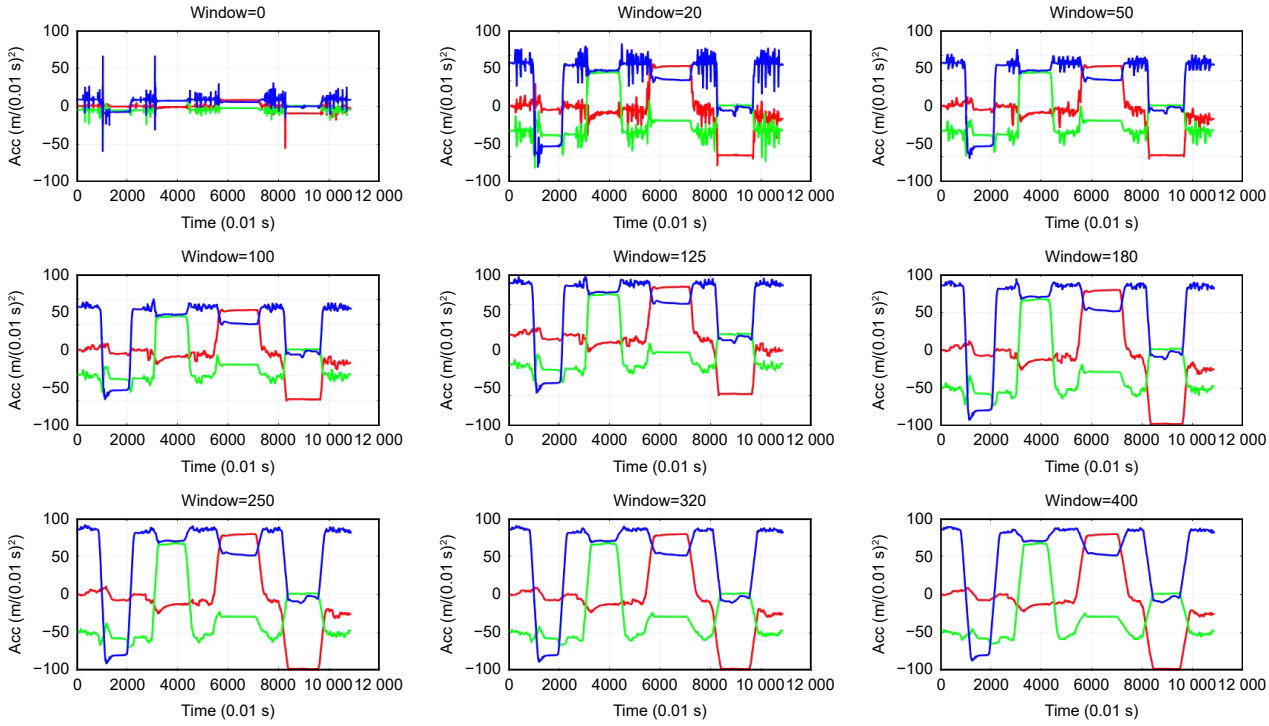

Fig. 5 Acceleration variation under different windows.

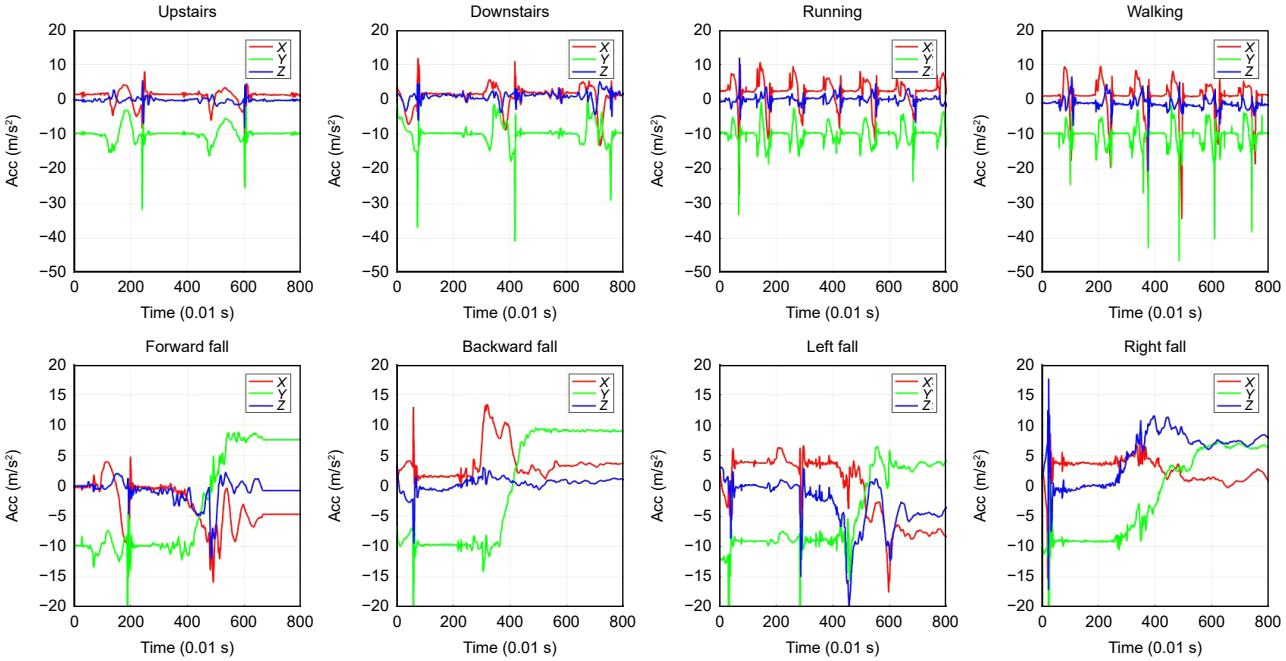

Fig. 6 Acceleration variation for each axis in different actions.

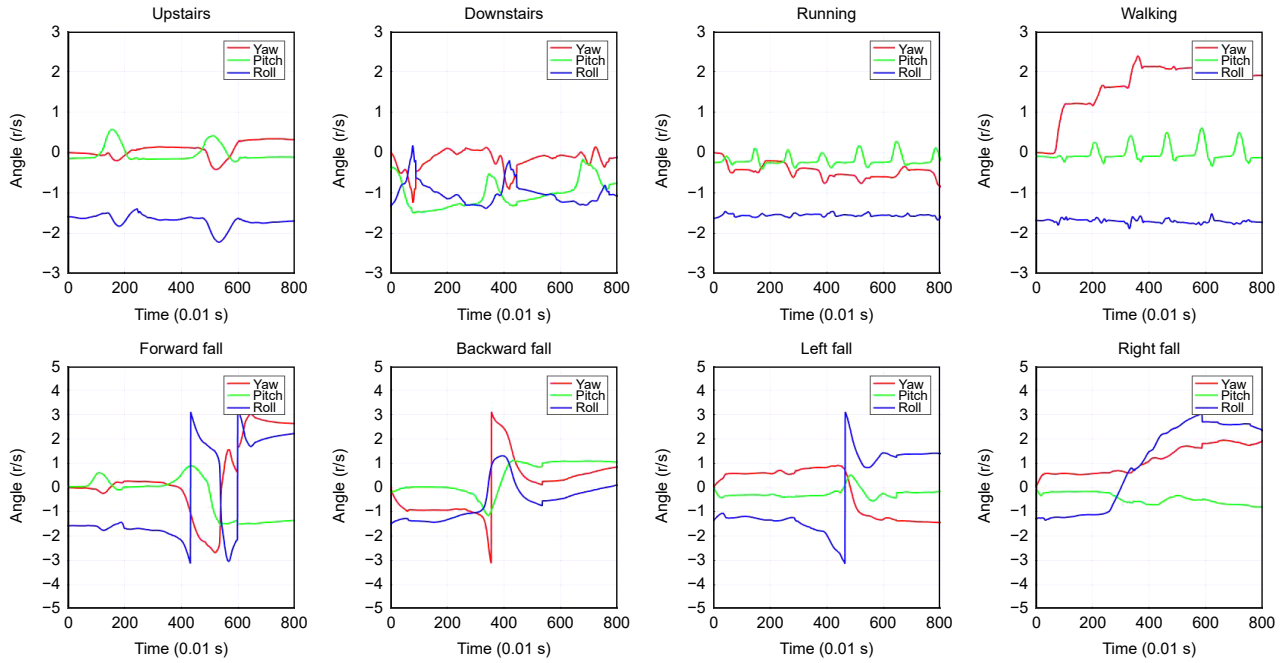

Fig. 7 Euler angle variation for each axis in different actions.

down stairs, running and walking are frequency and amplitude. However, the main difference between the waveforms of left, right, forward and backward falls is the step. In a word, the variations of the triaxial acceleration and Euler angular amplitude of these eight movements exhibit different forms over time. Therefore, we propose a feature method based on equal signal amplitude differences.

Within this work, a novel type of feature is introduced with the primary objective of enhancing precision during the training process. We extract acceleration and Euler angle features, respectively, and then put them into an SVM. In order to identify appropriate characteristics to distinguish falls from ADL, we analyzed the characteristics of the different activities. As previously mentioned, during normal

activities such as going stairs or walking, the data curves are smooth with small fluctuations. Instead, during fall events, the data fluctuations are volatile. Therefore, we adopt a novel features extraction method, equational signal magnitude variation (ESMV), to reflect the data fluctuations. The ESMV feature is defined as follows:

$$\mathrm{ESMV} = \arctan\left(\frac{y_{i+1} - y_i}{\Delta t}\right) \tag{9}$$

where the sample value y_i is the i-th sample, and Δt is the sample time difference.

For all training data from categories 1 to 8, where categories 1 to 4 are ADLs, and categories 4 to 8 are fall activities, acceleration and Euler angles are extracted as features for the SVM classifier. In this section, we establish classifiers by using angles. Through extensive experiments, we find that the best experimental results are obtained by setting nine classifiers, which are −90 degrees, −70 degrees, −50 degrees, −30 degrees, −10 degrees, 10 degrees, 30 degrees, 50 degrees, 70 degrees, and 90 degrees. Every training sample's acceleration feature matrix can be written as F_A:

$$F_A = \left(A_x, A_y, A_z\right)' = \begin{pmatrix} a_{x,1} & a_{x,2} & \cdots & a_{x,9} \\ a_{y,1} & a_{y,2} & \cdots & a_{y,9} \\ a_{z,1} & a_{z,2} & \cdots & a_{z,9} \end{pmatrix} \tag{10}$$

where A_x, A_y, and A_z represent the x, y, and z axes of acceleration, respectively; $a_{x,i}$, $a_{y,i}$, and $a_{z,i}$ indicate the number of ESMVs belonging to each classifier, respectively.

Each training sample's Euler angle feature matrix is written as F_E :

$$F_E = \left(E_x, E_y, E_z\right)' = \begin{pmatrix} e_{x,1} & e_{x,2} & \cdots & e_{x,9} \\ e_{y,1} & a_{y,2} & \cdots & e_{y,9} \\ e_{z,1} & e_{z,2} & \cdots & e_{z,9} \end{pmatrix} \tag{11}$$

where E_x, E_y, and E_z represent the x, y, and z axes of Euler angle, respectively; $e_{x,i}$, $e_{y,i}$, and $e_{z,i}$ indicate the number of ESMVs belonging to each classifier, respectively.

After the feature selection, the feature vectors of each training sample are expressed as follows:

$$F_{\mathrm{sum}} = \begin{pmatrix} F'_A & F'_B \end{pmatrix} = \begin{pmatrix} A_x & A_y & A_z & E_x & E_y & E_z \end{pmatrix} \tag{12}$$

All eight action samples' feature vectors are combined into one feature matrix in the manner described below:

$$F = \left(F_{1,\,\mathrm{sum}}, F_{2,\,\mathrm{sum}}, F_{3,\,\mathrm{sum}}, \ldots, F_{N,\,\mathrm{sum}}\right) \tag{13}$$

where N represents total samples.

Prior to SVM training and prediction, we normalize the feature vectors to ensure that all feature values fall within the [0, 1] range. These specifics are provided:

$$y = (y_{\max} - y_{\min}) * (x - x_{\min}) / (x_{\max} - x_{\min}) + y_{\min} \tag{14}$$

where the values of each column vector in F are represented by the biggest and smallest element values, respectively, by $x_{\max}$ and $x_{\min}$. Assign $y_{\max}$ and $y_{\min}$ values of 1 and 0, respectively.

Figures 8 and 9 show the data of acceleration and Euler angle features, respectively. In the controlled activity, except for the high degree of distinction between the running and walking features, a small portion of the eigenvalues between similar actions (e.g., up and down stairs) are more distinct, and most of the eigenvalues are close, which can easily lead to confusion. Figure 10 shows the data for the joint acceleration and Euler angle features (JAEFs), and since there are fewer eigenvalues that differ for a single feature, Fig. 10 combines the eigenvalues of both features. It is clear from Fig. 10 that there is a higher degree of differentiation between the combined acceleration and Euler angle features compared to the method using only a single feature, thus improving the

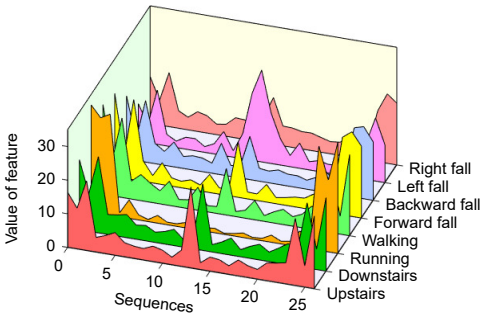

Fig. 8 Employing acceleration features.

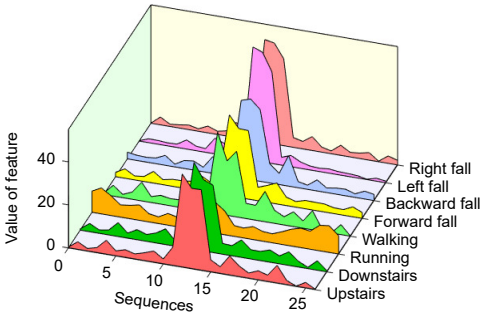

Fig. 9 Employing Euler angle features.

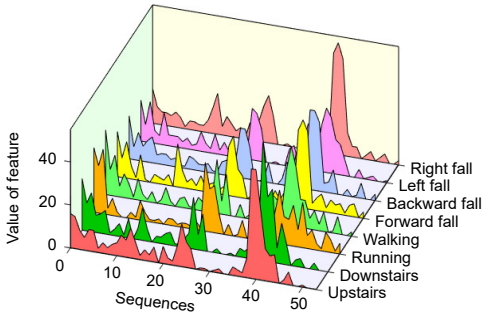

Fig. 10 Employing JAEF features.

classification accuracy.

When it comes to tackling the small sample, nonlinear, and high dimensional pattern recognition problem, the SVM classifier exhibits numerous distinct advantages. The primary principle of the SVM is to perform some nonlinear mapping on the input vector to transform it into a high-dimensional feature space.

It is worth mentioning that the SVM is essentially a regularized minimization problem, as shown following:

$$\min_{\xi}(\omega) = \frac{1}{2}\sum_{i=1}^{l}\omega_i^2 + C\sum_{i=1}^{l}\xi_i \tag{15}$$

$$y_i\left(\sum_{i=1}^{l}\omega_i\phi(x_i)+b\right) \geqslant 1-\xi_i \quad \forall i = 1,2,\ldots,l \tag{16}$$

where ξ_i is the slack variable and C stands for the penalty component. Furthermore, in order to avoid the explicit definition of the non-linear mapping, the kernel function is introduced.

The Lagrange function is established as

$$\begin{aligned} L(w,b,\alpha,\xi,\mu) = \frac{1}{2}\|w\|^2 + C\sum_{i=1}^{m}\xi_i + \\ \sum_{i=1}^{m}\alpha_i\left(1-\xi_i-y_i\left(w^{\mathrm{T}}x_i+b\right)\right) - \sum_{i=1}^{m}\mu_i\xi_i \end{aligned} \tag{17}$$

where $\alpha_i \geqslant 0$, $\mu_i \geqslant 0$ are Lagrange multipliers.

Let the partial derivative of $L(w,b,\alpha,\xi,\mu)$ with respect to w, b, α be zero, it yields

$$\begin{cases} w = \sum_{i=1}^{m}\alpha_i y_i x_i, \\ \sum_{i=1}^{m}\alpha_i y_i = 0, \\ C = \alpha_i + \mu_i \end{cases} \tag{18}$$

Substituting Eq. (18) into Eq. (17), we have

$$L(w,b,\alpha) = \sum_{i=1}^{m}\alpha_i - \frac{1}{2}\sum_{i=1}^{m}\sum_{j=1}^{m}\alpha_i\alpha_j y_i y_j x_i x_j \tag{19}$$

$$\sum_{i=1}^{m}\alpha_i y_i = 0, \quad \alpha_i \geqslant 0, \quad i = 1,2,\ldots,m \tag{20}$$

After solving α, according to Eq. (18), we can further obtain the values of w, and further find b, and then get the following model:

$$f(x) = w^{\mathrm{T}}x + b = \sum_{i=1}^{m}\alpha_i y_i x_i^{\mathrm{T}}x + b \tag{21}$$

The Karush-Kuhn-Tucker (KKT) conditions for the above process are given as

$$\begin{cases} \alpha_i \geqslant 0, \\ y_i f(x_i) \geqslant 1-\xi_i, \\ \alpha_i(y_i f(x_i) - 1 + \xi_i) = 0, \\ \log_i \geqslant 0, \mu_i\xi_i = 0 \end{cases} \tag{22}$$

Moreover, using Lagrange theory and quadratic programming strategies to solve the minimization problem. To model a real-world scenario for an internet application in the suggested architecture, we generate a feature matrix from the processed accelerations and Euler angles, and put it into SVM classification for continuous training, so as to obtain a better training framework. Then, the frame is extracted and the real-time motion data of the elderly is processed and transmitted to the model of the SVM classifier through Bluetooth to judge whether the elderly's activity is falling or daily life activities.

4 Expertmental Study

4.1 Experiment setup

Next, we will introduce the experimental process in a real scenario. Figure 11 shows the experimental scenario, which is on the 17th floor of Building B of the Science Education Building at Hefei University of

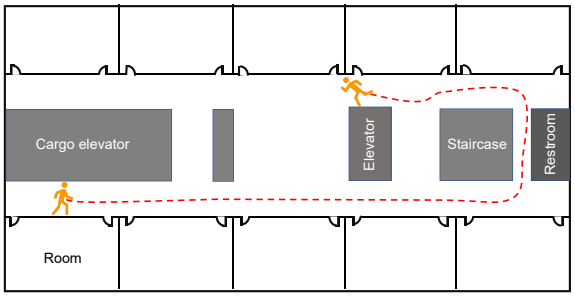

Fig. 11 Experimental areas.

Technology. We conducted a lot of experiments in the laboratory, hall, and corridor. Additionally, falling left, falling right, running, walking, falling ahead, falling backward, and climbing and descending stairs were taking into account. Besides, the 15 volunteers aged 20 to 27 years old, with heights ranging from 161 cm to 188 cm and weights ranging from 45 kg to 80 kg, carry out various activities. They are each in great health and do not have any physical ailments that might affect how they move.

To imitate activities that are similar to those carried out by seniors, they had to mimic the actions older adults take in the video clips. For the walking trials and fall trials, a subject completed each type of trial 50 times. The walking trials consisted of a minimum of two full gait cycles. Throughout the walking trials, the comprehensive sequence of activities, including running, walking, ascending, and descending stairs, is meticulously captured in the experimental data. Throughout the fall trials, each person performed 50 falls in the forward, backward, left, and right directions. At the same height, subjects landed on mattresses. Every reliable fall test result must have at least two complete walking motion data. Nearly 400 experimental trials were conducted overall.

A division was made within the experimental trials, creating a training subset and a testing subset. The training subset consisted of the complete set of experimental data obtained from eight subjects, while the remaining information from the other seven subjects was utilized for testing purposes.

4.2 Quality criteria

As an effective way to represent classification findings, this study focuses on indicators based on the confusion matrix,

$$\mathrm{CM} \equiv \begin{bmatrix} m_{11} & m_{12} & \dots & m_{1C} \\ m_{21} & m_{22} & \dots & m_{2C} \\ \vdots & \vdots & \ddots & \vdots \\ m_{C1} & m_{C2} & \dots & m_{CC} \end{bmatrix} \tag{23}$$

The expression represents the number of elements actually belonging to the i-th class but that are identified as belonging to the j-th class. In the context of our research, it is better to describe the term m_{ij} in terms of the total number of items m_i belonging to the i-th class. By denoting λ_{ij} as the ratio m_{ij}/m_i, it yields

$$\mathrm{CM} = \begin{bmatrix} \lambda_{11}m_1 & \lambda_{12}m_1 & \cdots & \lambda_{1C}m_1 \\ \lambda_{21}m_2 & \lambda_{22}m_2 & \cdots & \lambda_{2C}m_2 \\ \vdots & \vdots & \ddots & \vdots \\ \lambda_{C1}m_C & \lambda_{C2}m_C & \cdots & \lambda_{CC}m_C \end{bmatrix} \tag{24}$$

which is the Hadamard (elementwise) product of two matrices with the following expression as

$$\begin{bmatrix} \lambda_{11} & \lambda_{12} & \dots & \lambda_{1C} \\ \lambda_{21} & \lambda_{22} & \dots & \lambda_{2C} \\ \vdots & \vdots & \ddots & \vdots \\ \lambda_{C1} & \lambda_{C2} & \dots & \lambda_{CC} \end{bmatrix} \circ \begin{bmatrix} m_1 & m_1 & \dots & m_1 \\ m_2 & m_2 & \dots & m_2 \\ \vdots & \vdots & \ddots & \vdots \\ m_C & m_C & \dots & m_C \end{bmatrix} \tag{25}$$

The confusion matrix can be expressed as in the binary case, when $C = 2$, the classes are present as

$$\mathrm{CM} \equiv \begin{bmatrix} m_{11} & m_{12} \\ m_{21} & m_{22} \end{bmatrix} \tag{26}$$

One of the classes is typically referred to as the "Positive class", and the other as the "Negative class". Therefore, using this new terminology, the confusion matrix can now be represented as follows:

$$\mathrm{CM} \equiv \begin{bmatrix} m_{\mathrm{PP}} & m_{\mathrm{PN}} \\ m_{\mathrm{NP}} & m_{\mathrm{NN}} \end{bmatrix} \tag{27}$$

where the elements of this matrix m_{PP} means "True Positive (TP)"; m_{PN} means "False Negative (FN)"; m_{NP} means "False Positive (FP)"; and m_{NN} means "True Negative (TN)".

Consider a dataset $D = \{d_1, d_2, \dots, d_m\}$ with m elements, where d_k is the k-th element. The total number of positive m_{P} and negative m_{N} elements in D is equal to the total number of elements, that is, $m_{\mathrm{P}} + m_{\mathrm{N}} = m$. Furthermore, it is also true that the number of elements correctly classified in class P (m_{PP}), and the number of elements misclassified in that class P (m_{PN}), adds up to the number of elements in the positive class (m_{P}), that is, $m_{\mathrm{PP}} + m_{\mathrm{PN}} = m_{\mathrm{P}}$. Similarly, it can be stated that $m_{\mathrm{NP}} + m_{\mathrm{NN}} = m_{\mathrm{N}}$. The confusion matrix can therefore be written as

$$\mathrm{CM} = \begin{bmatrix} m_{\mathrm{PP}} & m_{\mathrm{P}} - m_{\mathrm{PP}} \\ m_{\mathrm{N}} - m_{\mathrm{NN}} & m_{\mathrm{NN}} \end{bmatrix} \tag{28}$$

This is also formulable using the ratios as

$$\mathrm{CM} = \begin{bmatrix} \lambda_{\mathrm{PP}}m_{\mathrm{P}} & \lambda_{\mathrm{PN}}m_{\mathrm{P}} \\ \lambda_{\mathrm{NP}}m_{\mathrm{N}} & \lambda_{\mathrm{NN}}m_{\mathrm{N}} \end{bmatrix} = \begin{bmatrix} \lambda_{\mathrm{PP}}m_{\mathrm{P}} & (1-\lambda_{\mathrm{PP}})m_{\mathrm{P}} \\ (1-\lambda_{\mathrm{NN}})m_{\mathrm{N}} & \lambda_{\mathrm{NN}}m_{\mathrm{N}} \end{bmatrix} \tag{29}$$

Additionally, use e_{P} and e_{N} to represent the total number of items in D that are assessed to be positive (despite their true class) and negative, respectively,

shown as

$$e_{\mathrm{P}} = m_{\mathrm{PP}} + m_{\mathrm{NP}} = \lambda_{\mathrm{PP}} m_{\mathrm{P}} + (1-\lambda_{\mathrm{NN}}) m_{\mathrm{N}} \tag{30}$$

$$e_{\mathrm{N}} = m_{\mathrm{NN}} + m_{\mathrm{PN}} = \lambda_{\mathrm{NN}} m_{\mathrm{N}} + (1-\lambda_{\mathrm{PP}}) m_{\mathrm{P}} \tag{31}$$

which means $e_{\mathrm{P}} + e_{\mathrm{N}} = m$. Figure 12 presents a summary of the confusion matrix definitions.

4.3 Experiment results

We conduct three comparable experiments utilizing three different sets of features: accelerations alone, Euler angles alone, and accelerations and Euler angles together. Results showed that the accuracy of recognition can be considerably increased by using accelerations and Euler angles as characteristics. Figure 13 shows the confusion matrix for fall activities and ADLs, employing the acceleration features. Figure 14 shows the confusion matrix for fall activities and ADLs, employing Euler angle features. Figure 15 shows the confusion matrix for fall accidents and ADLs, employing joint the acceleration and Euler angle features. The confusion matrix demonstrates that the chosen features function well in identifying the eight different sorts of activities.

		Predicted class: P	Predicted class: N	
Actual class	P	TP $\lambda_{\mathrm{PP}} m_{\mathrm{P}}$	FN $(1-\lambda_{\mathrm{PP}}) m_{\mathrm{P}}$	m_{P}
	N	FP $(1-\lambda_{\mathrm{NN}}) m_{\mathrm{N}}$	TN $\lambda_{\mathrm{NN}} m_{\mathrm{N}}$	m_{N}
		e_{P}	e_{N}	m

Fig. 12 Confusion matrix for binary classification.

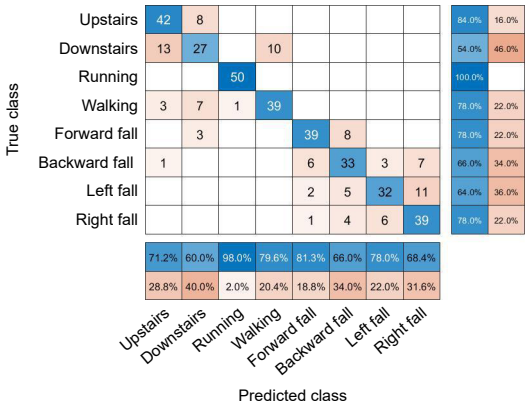

Fig. 13 Confusion matrix for fall activities and ADLs employing acceleration features.

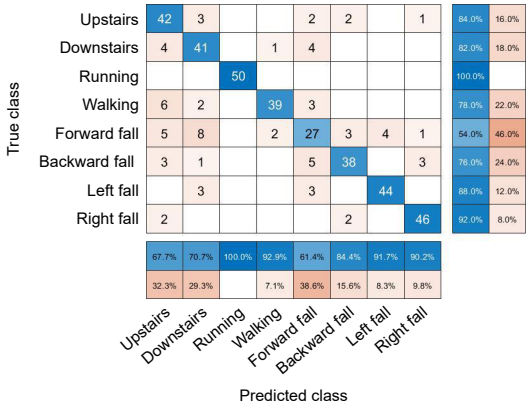

Fig. 14 Confusion matrix for fall activities and ADLs employing Euler angle features.

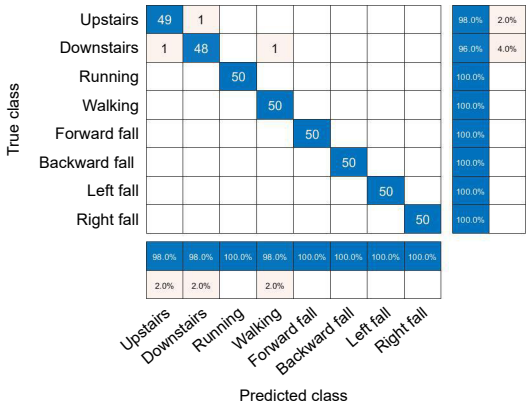

Fig. 15 Confusion matrix for fall activities and ADLs employing JAEF features.

Figures 16–18 show the comparison among equal-signal amplitude difference feature method, statistical feature method (SF)[33], and threshold method (TM)[34] in terms in precision, recall, and F1-score, respectively. To begin with, it can be seen from the figure that the traditional threshold-based method is significantly lower than our proposed method as well as the statistical feature-based method in precision, recall, and

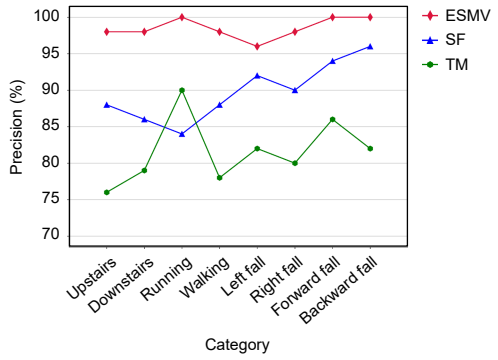

Fig. 16 Precision of different methods.

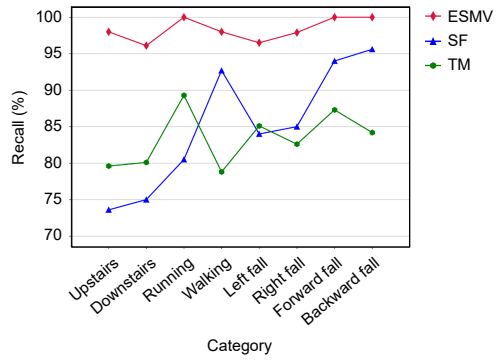

Fig. 17 Recall of different methods.

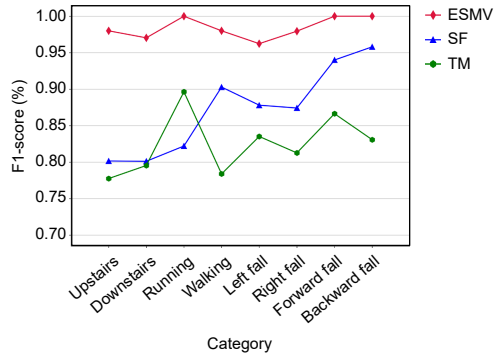

Fig. 18 F1-score of different methods.

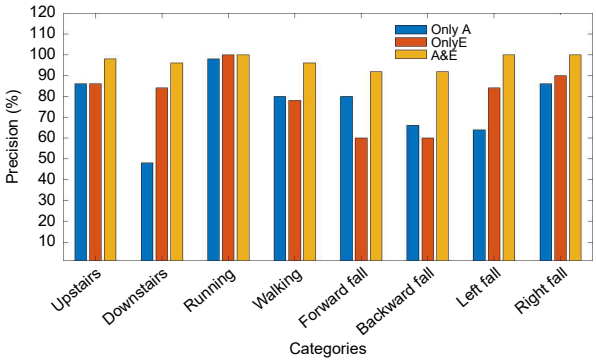

Fig. 19 Comparison chart of detection precision.

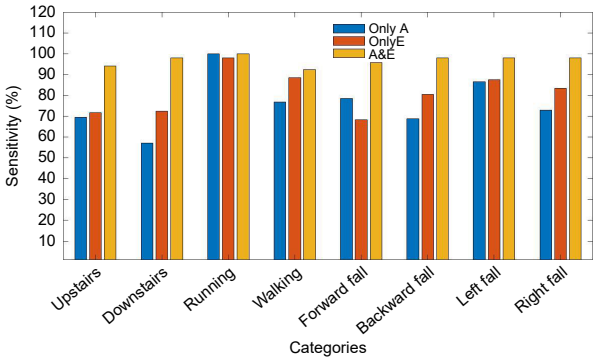

Fig. 20 Comparison chart of detection sensitivity.

F1-score. Next, according to data results, although the statistical feature-based method has higher accuracy for forward fall, backward fall, left-side fall, and right-side fall, there is no clear distinction between up and down stairs, running, and walking. To summarize, we find that the proposed feature method significantly outperforms the statistical feature method and the threshold method in terms of accuracy, recall, and F1-scores for the same dataset.

Human activities can be divided into eight groups using the SVM classifier. The results demonstrate that the approach is capable of accurately differentiating between various fall and ADLs kinds. Figures 19 and 20 compare the multi-feature-based method with two single-feature-based methods in precision and sensitivity. According to the results, the method using a single Euler angle feature and a single acceleration feature produces unsatisfactory results. However, the multi-feature method clearly outperforms the single-feature methods.

Through experimental verification, the method proposed in this paper has been proven to be effective. We conducted a series of experiments to evaluate the performance of this method in detecting falls in the elderly and compared it with other existing methods. The experimental results demonstrate that our method exhibits excellent performance in fall detection. By extracting multiple features, including combined acceleration and Euler angle features, our classifier is able to accurately identify fall behaviors. Compared to traditional methods, our approach shows significant improvements in sensitivity, precision, and classification accuracy. This method demonstrates good performance and has the potential for wide application in fall injury systems. We believe that this research will make important contributions to the health and safety of the elderly and provide valuable references for future related studies.

5 Conclusion

The present study devises and assesses a fall detection system for detecting pre-impact falls. This system leverages data concerning acceleration and angular velocity to extract relevant features. Following the selection of the classifying components, the SVM classifier is employed to categorize the data accurately. Drawing upon the results of feature selection, the incorporation of acceleration and angular velocity data proves to be pivotal in the classification of activities. The experimental findings indicate that utilizing

multiple features for fall detection yields an average sensitivity surpassing 96%. The combination of acceleration characteristics and Euler angles effectively reduces the occurrence of false alarms. The multi-feature-based approach demonstrates superior performance with an accuracy exceeding 98%, surpassing the previous single-feature-based techniques.

When considering precision, sensitivity, and specificity, the new method outperforms the prior single-feature-based approach. Despite certain limitations, a unique strategy for detecting falls before they happen and reducing potential harm is proposed. The remarkable accuracy and recall of this technique hold great potential for real-time pre-impact fall detection. Our aim is to enhance the flexibility of the angle classifier algorithm within the feature extraction algorithm, thereby enhancing the accuracy and robustness of the elderly fall detection system. In the future, we plan to combine video image and deep learning techniques to improve the accuracy and robustness of the system.

Acknowledgment

This work was supported by the National Natural Science Foundation of China (No. 61972131), and the National Key Research and Development Program (No. 2018YFB2100301).

References

[1] T. M. Gill, T. E. Murphy, E. A. Gahbauer, and H. G. Allore, The course of disability before and after a serious fall injury, *JAMA Inter. Med.*, vol. 173, no. 19, pp. 1780–1786, 2013.

[2] G. Bergen, M. R. Stevens, and E. R. Burns, Falls and fall injuries among adults aged 65 years-united states, 2014, *MMWR Morb. Mortal. Wkly. Rep.*, vol. 65, no. 37, pp. 993–998, 2016.

[3] T. Xu, Y. Zhou, and J. Zhu, New advances and challenges of fall detection systems: A survey, *Appl. Sci.*, vol. 8, no. 3, p. 418, 2018.

[4] B. Y. Su, K. Ho, M. J. Rantz, and M. Skubic, Doppler radar fall activity detection using the wavelet transform, *IEEE Trans. Biomed. Eng.*, vol. 62, no. 3, pp. 865–875, 2014.

[5] Y. Li, K. Ho, and M. Popescu, A microphone array system for automatic fall detection, *IEEE Trans. Biomed. Eng.*, vol. 59, no. 5, pp. 1291–1301, 2012.

[6] S. Kianoush, S. Savazzi, F. Vicentini, V. Rampa, and M. Giussani, Device-free RF human body fall detection and localization in industrial workplaces, *IEEE Internet Things J.*, vol. 4, no. 2, pp. 351–362, 2016.

[7] Y. Li, K. Ho, and M. Popescu, Efficient source separation algorithms for acoustic fall detection using a microsoft kinect, *IEEE Trans. Biomed. Eng.*, vol. 61, no. 3, pp. 745–755, 2013.

[8] V. Divya and R. L. Sri, Docker-based intelligent fall detection using edge-fog cloud infrastructure, *IEEE Internet Things J.*, vol. 8, no. 10, pp. 8133–8144, 2020.

[9] J. Liu and T. E. Lockhart, Development and evaluation of a prior-to-impact fall event detection algorithm, *IEEE Trans. Biomed. Eng.*, vol. 61, no. 7, pp. 2135–2140, 2014.

[10] T. R. Mauldin, M. E. Canby, V. Metsis, A. H. Ngu, and C. C. Rivera, SmartFall: A smartwatch-based fall detection system using deep learning, *Sensors*, vol. 18, no. 10, p. 3363, 2018.

[11] F. Hussain, F. Hussain, M. Ehatisham-ul Haq, and M. A. Azam, Activity aware fall detection and recognition based on wearable sensors, *IEEE Sens. J.*, vol. 19, no. 12, pp. 4528–4536, 2019.

[12] C. F. Lai, Y. M. Huang, J. H. Park, and H. C. Chao, Adaptive body posture analysis for elderly-falling detection with multisensors, *IEEE Intell. Syst.*, vol. 25, no. 02, pp. 20–30, 2010.

[13] H. Wang, D. Zhang, Y. Wang, J. Ma, Y. Wang, and S. Li, RT-Fall: A real-time and contactless fall detection system with commodity WiFi devices, *IEEE Trans. Mobile Comput.*, vol. 16, no. 2, pp. 511–526, 2016.

[14] W. Lu, M. C. Stevens, C.Wang, S. J. Redmond, and N. H. Lovell, Smart triggering of the barometer in a fall detector using a semi-permeable membrane, *IEEE Trans. Biomed. Eng.*, vol. 67, no. 1, pp. 146–157, 2019.

[15] L. Montanini, A. Del Campo, D. Perla, S. Spinsante, and E. Gambi, A footwear-based methodology for fall detection, *IEEE Sens. J.*, vol. 18, no. 3, pp. 1233–1242, 2017.

[16] T. de Quadros, A. E. Lazzaretti, and F. K. Schneider, A movement decomposition and machine learning-based fall detection system using wrist wearable device, *IEEE Sens. J.*, vol. 18, no. 12, pp. 5082–5089, 2018.

[17] M. Nyan, F. E. Tay, and E. Murugasu, A wearable system for pre-impact fall detection, *J. Biomech.*, vol. 41, no. 16, pp. 3475–3481, 2008.

[18] G. Shi, C. S. Chan, W. J. Li, K. S. Leung, Y. Zou, and Y. Jin, Mobile human airbag system for fall protection using mems sensors and embedded svm classifier, *IEEE Sens. J.*, vol. 9, no. 5, pp. 495–503, 2009.

[19] S. Shan and T. Yuan, A wearable pre-impact fall detector using feature selection and support vector machine, in *Proc. 10th IEEE Int. Conf. Signal Process*, Beijing, China, 2010, pp. 1686–1689.

[20] G. Wu and S. Xue, Portable preimpact fall detector with inertial sensors, *IEEE Trans. Neural Syst. Rehabil. Eng.*, vol. 16, no. 2, pp. 178–183, 2008.

[21] A. K. Bourke, K. J. O'Donovan, and G. Olaighin, The identification of vertical velocity profiles using an inertial sensor to investigate pre-impact detection of falls, *Med. Eng. Phys.*, vol. 30, no. 7, pp. 937–946, 2008.

[22] L. Gao, A. K. Bourke, and J. Nelson, A system for activity recognition using multi-sensor fusion, in *Proc. 33rd Annu. Int. Conf. IEEE Eng. Med. Biol. Soc*, 2011, pp. 7869–7872.

[23] M. Nyan, F. E. Tay, and M. Z. Mah, Application of motion analysis system in pre-impact fall detection, *J.*

Biomech., vol. 41, no. 10, pp. 2297–2304, 2008.
[24] C. Wang, L. Tang, M. Zhou, Y. Ding, X. Zhuang, and J. Wu, Indoor human fall detection algorithm based on wireless sensing, *Tsinghua Science and Technology*, vol. 27, no. 6, pp. 1002–1015, 2022.
[25] V. Vapnik, The nature of statistical learning theory, *Berlin, Germany*: *Springer*, 1999.
[26] S. Abbate, M. Avvenuti, F. Bonatesta, G. Cola, P. Corsini, and A. Vecchio, A smartphone-based fall detection system, *Pervasive Mob. Comput.*, vol. 8, no. 6, pp. 883–899, 2012.
[27] M. Yu, Y. Yu, A. Rhuma, S. M. R. Naqvi, L. Wang, and J. A. Chambers, An online one class support vector machine-based person-specific fall detection system for monitoring an elderly individual in a room environment, *IEEE J. Biomed. Health Inform.*, vol. 17, no. 6, pp. 1002–1014, 2013.
[28] V. R. Shen, H. Y. Lai, and A. F. Lai, The implementation of a smartphone-based fall detection system using a high-level fuzzy petri net, *Appl. Soft Comput. J*, vol. 26, pp. 390–400, 2015.
[29] R. M. Gibson, A. Amira, N. Ramzan, P. Casaseca-de-la Higuera, and Z. Pervez, Multiple comparator classifier framework for accelerometer-based fall detection and diagnostic, *Appl. Soft Comput. J*, vol. 39, pp. 94–103, 2016.
[30] L. Tong, Q. Song, Y. Ge, and M. Liu, HMM-based human fall detection and prediction method using tri-axial accelerometer, *IEEE Sens. J.*, vol. 13, no. 5, pp. 1849–1856, 2013.
[31] J. Liu and T. E. Lockhart, Development and evaluation of a prior-to-impact fall event detection algorithm, *IEEE Trans. Biomed. Eng.*, vol. 61, no. 7, pp. 2135–2140, 2014.
[32] L. Zhang, Q. Wang, H. Chen, J. Bao, J. Xu, and D. Li, Ard: Accurate and reliable fall detection with using a single wearable inertial sensor, in *Proc. 1st ACM Workshop on Mobile and Wireless Sensing for Smart Healthcare*, Sydney, Australia, 2022, pp. 13–18.
[33] Y. Wu, Y. Su, R. Feng, N. Yu, and X. Zang, Wearable-sensor-based pre-impact fall detection system with a hierarchical classifier, *Measurement*, vol. 140, pp. 283–292, 2019.
[34] J. Xie, K. Guo, Z. Zhou, Y. Yan, and P. Yang, Art: Adaptive and real-time fall detection using cots smart watch, in *Proc. 6th Int. Conf. Big Data Comput. Commun.* (*BIGCOM*), Deqing, China, 2020, pp. 33–40.

Li Zhang received the BS degree in applied mathematics from Anhui Normal University, Wuhu, China, in 1999, and the MS and PhD degrees in computational mathematics and computer science and technology from Hefei University of Technology, Hefei, China, in 2004 and 2009, respectively. From 2012 to 2013, she was a postdoctoral researcher in computer science and technology at Arizona State University, Phoenix, AZ, USA. She is currently a professor with School of Mathematics, Hefei University of Technology. Her current research interests include indoor localization, mobile computing, and Internet of Things.

Qiuyu Wang received the BS degree in applied mathematics from Anqing Normal University, Anqing, China, in 2019, and the ME degree from School of Mathematics, Hefei University of Technology. Her research interests include the Internet of Things.

Jingao Xu received the BE degree from School of Software, Tsinghua University, in 2017, and the PhD degree from School of Software, Tsinghua University, in 2022. He is currently a postdoctoral researcher in School of Software, Tsinghua University. His research interests include the mobile computing, edge computing, wireless localization, visual SLAM systems, and drone-based applications.

Yu-An Liu received the MS degree in control science and engineering from Anhui University of Technology, Ma'anshan, China, in 2022. He is currently working toward the PhD degree in mathematics from Hefei University of Technology, Hefei, China. His current research interests include networked control system and Internet of Things.

Huilin Chen received the BS degree in applied mathematics from Anqing Normal University, Anqing, China, in 2021. She is currently pursuing the master's degree with School of Mathematics, Hefei University of Technology. Her research interests include the Internet of Things.

Danyang Li received the BE degree in School of Software from Yanshan University in 2019 and the ME degree in School of Software from Tsinghua University in 2022. He is currently pursuing the PhD degree in School of Software, Tsinghua University. His research interests include Internet of Things and mobile computing.